11th International Symposium on Turbulence and Shear Flow Phenomena (TSFP11)
Southampton, UK, July 30 to August 2, 2019

Influence of wall-attached structures on the boundary of quiescent core region in turbulent pipe flow

Jongmin Yang
Department of Mechanical Engineering
KAIST
Daejeon 34141, Republic of Korea
Email : asyligo@kaist.ac.kr

Jinyul Hwang
Department of Mechanical Engineering
KAIST
Daejeon 34141, Republic of Korea
Email : j.yhwang@kaist.ac.kr

Hyung Jin Sung
Department of Mechanical Engineering
KAIST
Daejeon 34141, Republic of Korea
Email : hjsung@kaist.ac.kr

ABSTRACT

The entrainment phenomena of the quiescent core region in a turbulent pipe flow are examined by characterizing the tall wall-attached structures of the streamwise velocity fluctuations (u) extracted from direct numerical simulation data for Re_τ = 926. The quiescent core region is the uniform momentum zone with the highest streamwise velocity magnitude. The conditionally averaged turbulence statistics undergo an abrupt jump across the boundary of the core region, which indicates that there is a viscous shear layer at this interface, and that it is similar to the turbulent/non-turbulent interface. The turbulence statistics near the core boundary were obtained based on the projection area of the tall wall-attached structures that were extracted from the instantaneous flow field. Sharp changes in the turbulence statistics are evident; the magnitude of these changes increases with increases in the height (l_y) of the identified structures. We reconstructed the turbulence statistics by using the tall structures with $l_y+ > 100$, and found that the reconstructed profiles are remarkably similar to the turbulence statistics across the core boundary. These results confirm that the sudden changes in the averaged turbulence statistics and the modulation of v_n are associated with the instantaneous wall-attached structures that reach the core region.

INTRODUCTION

Wall-bounded turbulent flows are composed of several zonal structures with uniform streamwise momentum, i.e., uniform momentum zones (UMZs), as first reported by Meinhart & Adrian (1995). The UMZs are regions with a relatively uniform magnitude of instantaneous streamwise velocity ($\tilde{u}$), which leads to several step-like jumps in the wall-normal profile of $\tilde{u}$. The UMZs are located from the near-wall region to the outer region; the sizes of the largest UMZs are of the order of the outer length scale. Meinhart & Adrian (1995) used the term 'zones', to describe the instantaneous step-like jumps in streamwise velocity. Adrian et al. (2000) quantified the properties of UMZs by analyzing the probability density function (PDF) of the instantaneous streamwise velocity. These regions are demarcated by a thin viscous interface of strong shear containing groups of intense vortical structures (Adrian et al. 2000), and thus momentum transport arises across the edges of the UMZs. Recently, de Silva et al. (2016) found a log-linear increase with the Reynolds number in the number of UMZs and concluded that this phenomenon is associated with a hierarchical distribution of coherent structures, and thus is reminiscent of the attached-eddy hypothesis Townsend (1976). Moreover, Hwang & Sung (2018) showed the existence of wall-attached structures of the streamwise velocity fluctuations (u), which consist of multiple UMZs, contribute to the presence of the logarithmic layer. An exploration of UMZs is necessary to understand the turbulence statistics of instantaneous coherent structures.

Recently, Kwon et al. (2014) and Kwon (2016) modified the approach of Adrian et al. (2000) to the identification of UMZs in turbulent channel and pipe flows as a large central core regions with a uniform streamwise momentum. The turbulence in this core region is relatively weak and thus this region was designated the quiescent core. Although the quiescent core region is not identical to the irrotational flow in turbulent boundary layers, the boundary of the core region has significant structure and there is a sudden change in the turbulence statistics at the core boundary, as found for the turbulent/non-turbulent interface (TNTI). A TNTI that demarcates the turbulent and non-turbulent regions arises in many flows such as turbulent boundary layers, jets, and wakes. Such interfaces are significantly contorted and convoluted by turbulent eddies. The irrotational fluid is entrained into the turbulent region and the turbulent region spreads into the non-turbulent region. The dynamical process across the TNTI, known as entrainment, has an essential role in the transport of mass, momentum, and energy. However, it is not clear whether the dynamical process at the boundary of the quiescent core region has a direct impact on the mixing and reaction rates in the central region of the internal flow.

In the early experimental work of Corrsin & Kistler (1955), a laminar superlayer was found, for which the propagation of the interface is governed by the viscous diffusion between the

turbulent and non-turbulent regions of free shear flows. This laminar superlayer means that there is a finite jump in the velocity (i.e., there is a peak in the vorticity) across the interface. As suggested by Corrsin & Kistler (1955), the entrainment process is governed by small-scale motions that nibble at the interface Westerweel et al. (2009). In addition, the local entrainment velocity (v_n) obtained from the enstrophy transport equation shows that the viscous contribution is dominant and that the magnitude of the velocity is on the order of the Kolmogorov velocity scale (Holzner & Lüthi 2011). On the other hand, large-scale motions are also associated with the entrainment process. Engulfment processes in which the non-turbulent fluid is ingested by the turbulent region are associated with large-scale instabilities such as bulges or valleys in the outer regions Townsend (1976). Brown & Roshko (1974) concluded that there is a relationship between the entrainment and the large-scale coherent structures in the plane mixing layer. In addition, Kovasznay et al. (1970) found that the large-scale motions extending from the wall are related to the geometry of the TNTI. Although viscous diffusion through small-scale motions is the dominant entrainment process Westerweel et al. (2009), the global rate of entrainment is determined by the large-scale engulfing motions (Holzner & Lüthi 2011; Chauhan et al. 2014). Moreover, the geometries of TNTIs exhibit fractal characteristics that enhance the effective surfaces of turbulent fluids (Chauhan et al. 2014). In other words, the interfacial dynamics is characterized by multi-scale motions, which suggests that the transport process across the interface is a consequence of the correlations between small- and large-scale motions. Thus, it is important to explore the relationship between the small- and large-scale motions that contribute to the entrainment process.

A finite jump in the mean streamwise velocity has been observed at the boundary of the quiescent core region (Kwon et al. 2014). In addition, there is a positive peak in the spanwise vorticity at the core boundary, which indicates the presence of a high shear region. The thickness of the shear region is $0.015h$ (where h is the channel half-height), which is comparable to that reported for turbulent boundary layers (Chauhan et al. 2014). A high population density of prograde spanwise vortices was observed in the vicinity of the core boundary and these vortices were found to contribute significantly to the total mean shear (Yang et al. 2016). These observations confirm the presence of small-scale motions and the associated entrainment phenomena along the core boundary. As is the case for the TNTI, large-scale motions also influence the geometry of the quiescent core region (Yang et al. 2016) and are responsible for the turbulence kinetic energy and the Reynolds shear stress. Moreover, the distributions of the spanwise vortical structures depend on the shape of the core boundary (Yang et al. 2016), which implies that there is a relationship between the small- and large-scale motions. Wolf et al. (2012) showed that for a turbulent jet the magnitude of the local entrainment velocity, which is dominated by the small diffusive scales, varies with the shape of the TNTI. Since the shape of the core boundary is determined by the large-scale structures that reach the core region, the local entrainment velocity is likely to be modulated by these structures. Thus, there is great interest in exploring the relationship between the large-scale motions and the local entrainment velocity at the core boundary in order to obtain insights into the multi-scale nature of the interfacial dynamics in internal flows.

To extract the large-scale motions near the core boundary from our data, we explored the wall-attached structures of the streamwise velocity fluctuations (u). These structures are self-similar with respect to their heights (l_y) and exhibit hierarchical characteristics associated with multiple UMZs (Hwang & Sung 2018). These structures are closely related to bulges at the TNTI (Kovaszany et al. 1970) because they extend to the outer region. Moreover, the statistics for wall turbulence can be expressed as an accumulation of a hierarchical distribution of UMZs. Since the wall-attached structures are composed of multiple UMZs, it is essential to examine the tall attached structures near the core boundary in order to understand the sudden jump in the turbulence statistics and the global entrainment rates at the edge of the quiescent core region

The objective of the present study was to explore the influence of the wall-attached u structures on the quiescent core boundary in a turbulent pipe flow. We analyzed the DNS data of a pipe flow with $Re_\tau = 926$. First, we identified the core region with a high uniform streamwise momentum by examining the PDF of the modal velocity. Then, we extracted the tall attached structures near the interface from the instantaneous flow field. Finally, we reconstructed the turbulence statistics near the core interface by using the tall attached structures in order to determine how the attached structures contribute to the step-like jumps in turbulence statistics observed in the vicinity of the core interface.

NUMERICAL SIMULATION

In the present study, we used the DNS data of a turbulent pipe flow with $Re_\tau = 926$ (Ahn et al. 2013). The fully-developed turbulent pipe flow was numerically simulated with the Navier–Stokes equations and the continuity equation in cylindrical coordinates. The governing equations were non-dimensionalized by the centerline velocity (U_{CL}) and the pipe radius (R). The velocity and pressure were decomposed by using the fractional step method (Kim et al. 2002). The Reynolds number based on the pipe diameter (D) and the bulk velocity (U_b) was 53000. Periodic boundary conditions were adopted in the streamwise and azimuthal directions of the pipe and the no-slip condition was employed for the velocity components at the wall. The centerline velocities were obtained as the average velocities of the corresponding component across the centerline. In this approach, the axial length of the computational domain has a length of $10\pi R$. The number of grids is 4097 × 301 × 1025 in the streamwise (x), radial (r), and azimuthal (θ) directions, u_x, u_r, and u_θ are the corresponding velocity components, ω_x, ω_r, and ω_θ are the corresponding vorticity components, respectively. The Cartesian coordinate expressions are defined as follows: the wall-normal direction is given by $y = 1 - r$ and the spanwise direction by $z = r\theta$; the corresponding velocities are expressed as $\tilde{u} = u_x$, $\tilde{v} = -u_r$, and $= u_\theta$. The grid resolutions in the streamwise and azimuthal directions are $\Delta x^+ = 6.84$, $\Delta(R\theta)^+ = 5.73$ in wall units, respectively. The sampling time is $\Delta t U_{CL}/R = 0.01$, and the maximum and minimum spacings in the radial directions (Δy^+) are 0.334 and 9.244, respectively. Details of the validation are provided in Ahn et al. (2013). In the present study, we used a total of 1224 instantaneous flow fields so that the total time span is approximately 12100 viscous time units.

DETECTION OF THE QUIESCENT CORE INTERFACE

We examined the probability density function (PDF) of the streamwise velocity to identify the quiescent core (Kwon et al. 2014). The PDF of the streamwise velocity can be used to find

an appropriate threshold for the interface of the quiescent core, which is defined as a region where the streamwise velocity is relatively high and uniform. Figure 1(a) shows an instantaneous streamwise velocity field. Note the relatively uniform magnitude of ũ along the wall-normal direction. The corresponding PDF of $\tilde{u}$ is shown in Fig. 1(b), which was obtained by using 1.2R as the streamwise domain length of the subzone in the turbulent pipe flow. As shown in Fig. 1(b), there are two local maxima: one in a high velocity region ($\tilde{u} \approx U_{CL}$) and the other in a lower velocity region ($\tilde{u} \approx 0.8U_{CL}$). The PDF of the instantaneous streamwise velocity shows that there are two UMZs. The local maxima in the PDF of the streamwise velocity are known as 'modal velocities'. Each modal velocity corresponds to a UMZ in the selected subzone. However, the number of modal velocities is sensitive to the selection of the streamwise domain length of the subzone (Adrian et al. 2000; Kwon et al. 2014).

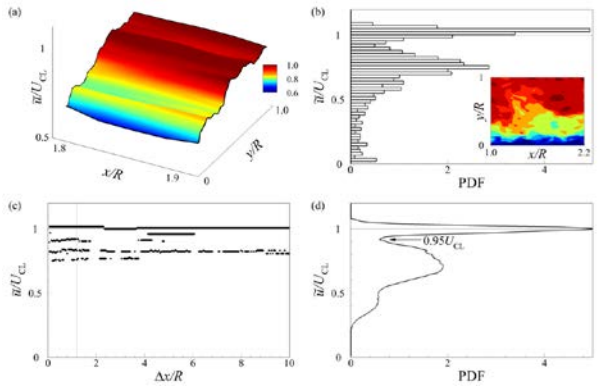

Figure 1. (a) 3D-Contour representation of the instantaneous streamwise velocity for 1.8 < x/R < 1.9 and 0 < y/R < 1. (b) The PDF of the instantaneous streamwise velocity was constructed by using 1.2R as the streamwise domain length of the subzone (inset). (c) The distribution of the modal velocities as a function of the streamwise domain length of the subzone (Δx). (d) The PDF of the modal velocities obtained from all the instantaneous flow fields with Δx = 1.2R.

Figure 1(c) shows the distribution of the modal velocities at a given streamwise domain length of the subzone (Δx). As can be seen in this figure, the modal velocity of the UMZ varies with Δx. Although the number of modal velocities decreases with increases in Δx, the modal velocity with the highest speed (i.e., $\tilde{u} \approx U_{CL}$) is observed for all Δx, as was reported for a turbulent channel flow (Kwon et al. 2014). Another important parameter is the bin size of the PDF since the number of modal velocities depends on the bin size. As the bin size increases, the total number of detected UMZs decreases gradually (results not shown here). However, the highest modal velocity at $\tilde{u} \approx U_{CL}$ is present regardless of the bin size, so this is a robust feature of this method for identifying the UMZ by using the PDF. In the present study, we employed a streamwise subzone length of 1.2R and a bin size of approximately 0.5u_τ Kwon et al. (2014).

Figure 1(d) shows the PDF of the modal velocity obtained from all the instantaneous flow fields. The dominant peak is at $\tilde{u} = U_{CL}$, which means that a UMZ is present in the core region of the pipe flow. The interface of the core can be identified from the local minima in the PDF of the modal velocity. We found that the core interface is located around $\tilde{u} = 0.95U_{CL}$, which is consistent with the location of the core interface in channel flows (Kwon et al. 2014; Yang et al. 2016).

TALL ATTACHED *u* STRUCTURES

To extract the u structures near the boundary, we considered the connected nodes that satisfy the following equation:

$$u(x,y,z,t) > \alpha u_{rms}(y) \text{ or } u(x,y,z,t) < -\alpha u_{rms}(y), \quad (1)$$

where $u_{rms}(y)$ is the root mean square value of the streamwise velocity fluctuations that depends on the wall-normal distance and α is the threshold value. Here, the connected nodes were identified by using the connectivity rule (Lozano-Duran et al. 2012; Hwang & Sung 2018), i.e., as the contiguous points of u satisfying equation (1) among the six orthogonal neighbors in cylindrical coordinates at a given node. The clusters of negative and positive fluctuations satisfying equation (1) can be denoted as low- and high-speed structures, respectively. Hwang & Sung (2018) and Hwang & Sung (2019) showed that the u clusters can be classified into wall-attached and wall-detached structures. In particular, the wall-attached clusters are self-similar with respect to their height (l_y) and exhibit an inverse power-law distribution (i.e., PDF ~ l_y^{-1}), as is reminiscent of Townsend's attached eddies. In the present study, we focused on the tall wall-attached structures of u ($l_y \sim O(R)$) that extend to the boundary of the core region, and were able to measure velocity information that contains within the object near the core boundary. The threshold value α was chosen based on the percolation behavior of u clusters (Hwang & Sung 2018; Hwang & Sung 2019). The percolation theory describes the connectivity between randomly distributed nodes, and has been previously used to analyze the three-dimensional structures of the vortex and the Reynolds shear stress Lozano-Duran et al. (2012).

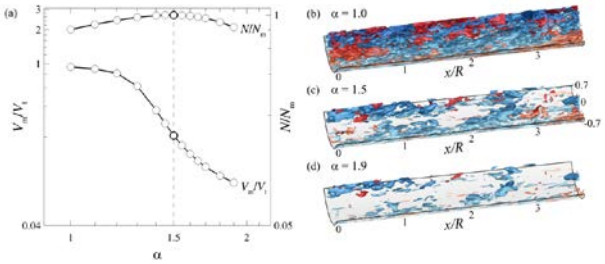

Figure 2. (a) Percolation diagram for the identified structures. Isosurfaces of the identified structures in the instantaneous flow field when (b) α = 0.5, (c) 1.3, and (d) 3.0. The blue and red isosurfaces are the low- and high-speed structures respectively.

Figure 2(a) shows the variations with α in the volume of the largest identified structure (V_m) and in the total number of identified structures (N). V_m and N are normalized by the total volume of the structures (V_t) and the maximum number of objects (N_m) respectively. As α increases, V_m/V_t decreases due to the loss of the connectivity among points, which is evident in Figs. 2(b–d). There is a peak at α = 1.5 in N/N_m. New clusters are identified and merged simultaneously according to α and the generation of clusters becomes dominant as α approaches 1.5, whereas N/N_m decreases for α > 1.5 because the merging of the identified objects is dominant. In the present study, we chose the threshold value α = 1.5. At α = 1.5, the total number

of identified structures is maximum and the volume changes significantly when the percolation crisis occurs.

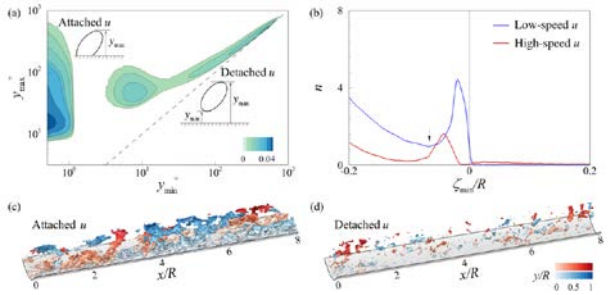

Figure 3. (a) The number of clusters per unit wall-parallel area ($= 2\pi RL_x$) as a function of y_{min} and y_{max}. (b) The population densities of the wall-attached low-speed (blue) and high-speed (red) structures as functions of ζ_{min}. ζ_{min} is the minimum wall-normal distance of the object from the core boundary. The arrow denotes $\zeta_{min} = -0.066R$ ($\approx 60\nu/u_\tau$). Isosurfaces of the (c) wall-attached and (d) wall-detached structures. The red and blue isosurfaces correspond to positive and negative fluctuations respectively, and the brightness of the color indicates the distance from the wall.

Next we explored the minimum and maximum wall distances (y_{min} and y_{max}) of each object to extract the wall-attached structures of u. Figure 3(a) shows the population density of the identified structures as a function of y_{min} and y_{max}. Here, the contour level indicates the number of objects per unit wall-parallel area ($= 2\pi RL_x$). As shown in Fig. 3(a), the identified structures can be classified into two groups, i.e., a wall-attached ($y_{min} \approx 0$) group or a wall-detached ($y_{min} > 0$) group. Figure 3(c) and (d) show examples of wall-attached and wall-detached structures in the instantaneous flow field. It is evident that most of the detached objects are very tiny. On the other hand, the wall-attached structures extend from the near-wall region to the outer region; note that some of them have large volumes and reach the pipe center. Next, we examined the wall-attached structures that are correlated with the characteristics of the core boundary.

Figure 3(b) shows the population density of wall-attached low-speed (blue) and high-speed (red) structures according to ζ_{min}. ζ_{min} is the minimum wall-normal distance of the identified object from the core boundary. Inside the core region ($\zeta_{min} > 0$), the population density is close to zero. The absence of such turbulent structures is related to the low turbulence intensity inside the core region. On the other hand, the population density increases sharply near the core boundary: there are two peaks at $\zeta_{min} \approx 0.02R$ ($= 18.5\nu/u_\tau$) and $0.04R$ ($= 37\nu/u_\tau$) for low- and high-speed structures respectively. This result indicates that most of the wall-attached structures are located in the non-core region and that there is additional weighting for the tall wall-attached structures that extend to the core boundary. Moreover, the peak value of the low-speed structures is more than twice that of the high-speed structures, which indicates that the low-speed structures are concentrated in the vicinity of the core interface. In other words, the turbulence statistics near the interface are likely to be affected by the wall-attached structures, and thus the entrainment phenomena around the interface are also correlated with the wall-attached structures in the vicinity of the core interface. In the following section, we further examine these structures by focusing on the objects with $\zeta_{min} > -0.066R$ ($\approx -60\nu/u_\tau$), where the population density of the low-speed structures is minimum (as indicated by the vertical dashed line in Fig. 3b).

EFFECTS OF WALL-ATTACHED STRUCTURES ON THE BOUNDARY OF THE QUIESCENT CORE

In this section, we analyze the turbulence statistics across the core boundary according to the height of the wall-attached structures ($l_y = y_{max}$). Here, the flow statistics are conditionally averaged in the vicinity of the projection area of the identified objects onto the core boundary. Figure 4(a) shows the conditional averages of the streamwise velocity ($\langle\tilde{u}_a\rangle$) with respect to l_y. As can be seen in this figure, all the profiles collapse well above the core boundary whereas there is a variation in the non-core region ($\zeta < 0$). The magnitude of $\langle\tilde{u}_a\rangle$ decreases with increasing l_y, which indicates that the velocity jump across the core boundary is enhanced for taller structures. In other words, the strong shear layer near the tall structures transfers momentum significantly. In addition, the lower magnitude of $\langle\tilde{u}_a\rangle$ is associated with the dominance of the intense low-speed structures beneath the core boundary (Fig. 3b) because the low-speed structures are composed of points with negative u and the taller structures contain lower values of u. The streamwise and wall-normal components of the turbulence intensity and the Reynolds shear stress are shown in Figs. 4(b–d). The Reynolds stresses in the non-core region vary significantly with l_y since the taller structures carry high magnitudes of the turbulence intensity.

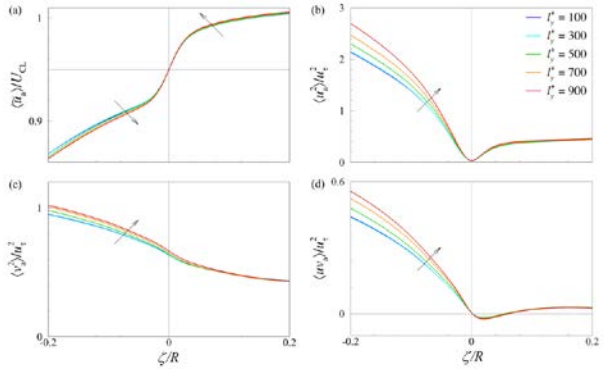

Figure 4. Conditional averages of (a) the streamwise velocity, (b) the streamwise turbulence intensity, (c) the wall-normal turbulence intensity, and (d) the Reynolds shear stress contained within the projection area of the wall-attached structures as a function of ζ. The heights of the wall-attached structures vary from $l_y^+ = 100$ to $l_y^+ = 900$. The horizontal line in (a) is $\tilde{u} = 0.95U_{CL}$

The growth of the wall-attached structures enhances the shear layer at the interface, and amplifies the entrainment governed by the viscous diffusion at the interface. To determine the structural relationships between the attached u structures and the interface, the conditional statistics were reconstructed by superposing the profiles in Fig. 4,

$$\langle\tilde{u}_{as}(\zeta)\rangle = \frac{\sum_{l_y} n_s(l_y)\langle\tilde{u}_a(\zeta, l_y)\rangle}{\sum_{l_y} n_s(l_y)}, \qquad (3)$$

where $\langle \tilde{u}_a \rangle$ is the conditional average of the streamwise velocity shown in Fig. 4 and n_s is the population density of wall-attached structures with respect to l_y. Figure 5 shows the reconstructed conditional profiles acquired by weighting the relative probability of the structures to the corresponding profiles. The solid lines and circles represent the mean conditional statistics across the interface and the reconstructed statistics, respectively. The reconstructed velocity, the turbulence intensity, and the Reynolds shear stress are both in good agreement with the mean conditional statistics. These results indicate that the attached *u* structures can be used to generate the flow statistics across the interface and that the wall-attached structures can be used to analyze the entrainment originating at the interface.

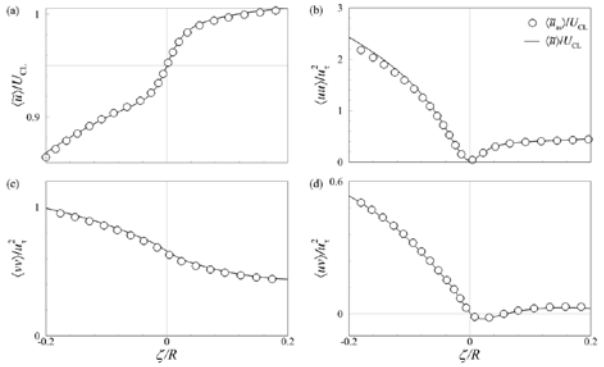

Figure 5. The conditional profiles (lines) in the mean conditional statistics and the reconstructed profiles (circles) obtained from equation (3): (a) the streamwise velocity, (b) the streamwise turbulence intensity, (c) the wall-normal turbulence intensity, and (d) the Reynolds shear stress.

CONCLUSIONS

We have analyzed the entrainment phenomena of a quiescent core region in a turbulent pipe flow with Re_τ = 926 by focusing on the wall-attached structures of *u*. The quiescent core region was identified by using the PDF of the streamwise modal velocity, which shows the presence of a UMZ with the highest magnitude velocity at the center of the pipe. The boundary demarcating the core was defined as the isosurface level $\tilde{u} = 0.95U_{CL}$, which is consistent with the core region in the turbulent channel flow. To explore the influence of the large-scale structures, we identified the wall-attached structures of *u* in the instantaneous flow field. There is a dominant peak in the population density of the wall-attached structures in the vicinity of the core boundary ($\zeta^+ < 60$). Furthermore, we conditionally averaged the streamwise velocity near the core boundary based on the projection area of the wall-attached structures. Regardless of the heights (l_y) of the identified structures, an abrupt change is evident. The velocity difference across the core boundary increases with increasing l_y, which indicates that the magnitude of the shear layer is enhanced when tall attached structures extend near to the pipe center. For the Reynolds stresses, the profiles collapse well within the core region whereas the profiles are shifted upwards with l_y within the core region. Finally, we reconstructed the turbulence statistics across the core boundary through the superposition of the flow statistics over $100 < l_y^+ < 900$. The reconstructed profiles are consistent with the conditional averages of the turbulence statistics across the core boundary.

ACKNOWLEDGEMENTS

This study was supported by a grant from the National Research Foundation of Korea (No. 2019M3C1B7025091), and partially supported by the Supercomputing Center (KISTI).

REFERENCES

Adrian, R.J., Meinhart, C.D., Tomkins, C. D., 2000, "Vortex organization in the outer region of the turbulent boundary layer", *Journal of Fluid Mechanics*, Vol. 422, pp. 1-54.

Ahn, J., Lee, J. H., Jang, S. J., Sung, H. J. 2013, "Direct numerical simulations of fully developed turbulent pipe flows for Re_τ = 180, 544 and 934", *International Journal of Heat Fluid Flow*, Vol. 44, pp. 222-228

Brown, G., Roshko, A. 1974, "On density effects and large structure in turbulent mixing layers", *Journal of Fluid Mechanics*, Vol. 64, pp. 775-816

Chauhan, K., Philip, J., de Silva, C. M., Hutchins, N., Marusic, I. 2014, "The turbulent/non-turbulent interface and entrainment in a boundary layer", *Journal of Fluid Mechanics*, Vol. 742, pp. 119-151

Corrsin, S., Kistler, A. L. 1955, "Free-stream boundaries of turbulent flows", NACA report, 1244

de Silva, C. M., Hutchins, N., Marusic, I, 2016, "Uniform momentum zones in turbulent boundary layers". *Journal of Fluid Mechanics*, Vol. 786, pp. 309-331

Holzner, M., Lüthi, B. 2011, "Laminar superlayer at the turbulence boundary", *Physics Review. Letters*, Vol. 106, 134503

Hwang, J., Sung, H. J. 2018, "Wall-attached structures of velocity fluctuations in a turbulent boundary layer", *Journal of Fluid Mechanics*, Vol. 856, pp. 958-983

Hwang, J., Sung, H. J. 2019, "Wall-attached clusters for the logarithmic velocity law in turbulent pipe", *Journal of Fluid Mechanics*, In press

Kim, K., Baek, S. -H., Sung, S. J. 2002, "An implicit velocity decoupling procedure for the incompressible Navier-Stokes equation", *International Journal for Numerical Methods in Fluids*, Vol. 38, pp. 125-138

Kovasznay, L. S. G., Kibens, V., Blackwelder, R. F. 1970, "Large-scale motion in the intermittent region of a turbulent boundary layer", *Journal of Fluid Mechanics*, Vol. 41, pp. 283-325

Kwon, Y. S., Philip, J., de Silva, C. M., Hutchins, N., Monty, J. P. 2014, "The quiescent core of turbulent channel flow", *Journal of Fluid Mechanics*, Vol. 751, pp. 228-254

Lozano-Duran, A., Flores, O., Jiménez, J. 2012, "The three-dimensional structure of momentum transfer in turbulent channels", *Journal of Fluid Mechanics*, Vol. 694, pp. 100-130

Meinhart, C. D., Adrian, R. J. 1995, "On the existence of uniform momentum zones in a turbulent boundary layer", *Physics of Fluid*, Vol. 7, 694

Townsend, A. A. 1976, "The structure of turbulent shear flow", Cambridge university press.

Westerweel, J., Fukushima, C., Pedersen, J. M., Hunt, J. C. R. 2009, "Momentum and scalar transport at the turbulent/non-turbulent interface of a jet", *Journal of Fluid Mechanics*, Vol. 631, pp. 199-230

Wolf, M., Lüthi, B., Holzner, M., Krug, D., Kinzelbach, W., Tsinober, A. 2012, "Investigations on the local entrainment velocity in a turbulent jet", *Physics of Fluid*, Vol. 24, 105110

Yang, J., Hwang, J., Sung, H. J. 2016, "Structural organization of the quiescent core region in a turbulent channel flow", *International Journal of Heat Fluid Flow*, Vol. 62, pp. 455-463